2007 IEEE International Conference on
Robotics and Automation
Roma, Italy, 10-14 April 2007

Stability Boundary for Haptic Rendering: Influence of Damping and Delay*

Jorge Juan Gil and Emilio Sánchez
CEIT and TECNUN
University of Navarra
P°Manuel Lardizábal 15, 20018 San Sebastián, Spain
jjgil@ceit.es

Thomas Hulin, Carsten Preusche and Gerd Hirzinger
German Aerospace Center - DLR
Institute of Robotics and Mechatronics
Münchner Str. 20, 82234 Oberpfaffenhofen, Germany
Thomas.Hulin@dlr.de

***Abstract*— The influence of viscous damping and delay on the stability of haptic systems is studied in this paper. The stability boundaries have been found by means of different approaches. Although the shape of these stability boundaries is quite complex, a new linear condition which summarizes the relation between virtual stiffness, viscous damping and delay is proposed. This condition is independent of the mass of the haptic device. The theoretical results are supported by simulations and experimental data using the DLR Light-Weight Robot.**

***Index Terms*— Haptic systems, Discrete-time systems, Stability, Time delay**

I. INTRODUCTION

A haptic interface can be used to link a human operator to a virtual environment in such way that the user is able to perceive the scene with the sense of touch. The ability of perceiving contact forces of virtual environments is essential in many industrial applications: virtual prototyping [1] and maintainability analysis [2], [3], surgery training [4], [5], driving simulators [6], etc. An elementary prerequisite for all these applications is to preserve stability. This paper studies the stability conditions of haptic systems and presents a relation between virtual stiffness, viscous damping and delay.

Section II presents a mathematical model of haptic systems and Section III summarizes previous stability and passivity conditions for such systems. In Section IV a new stability condition is presented. The validity of this condition is verified in sections V-VIII by four different ways. Section IX discusses the validity of the linear stability condition. Important conclusions are stated in Section X.

II. SYSTEM DESCRIPTION

From the control point of view, a haptic system is a sampled-data controlled mechatronic device. Fig. 1 shows the model of the haptic device colliding against a virtual wall with delay t_d. This time delay can be the sum of several effects: computations, communications, etc. The interface has a mass m, a physical damping b and a Coulomb friction c. A

*This work has been supported in part by the EU Government, Enactive Network of Excellence, project number IST-2002-002114; and the Basque Government, mobility program MV-2006-1-6.

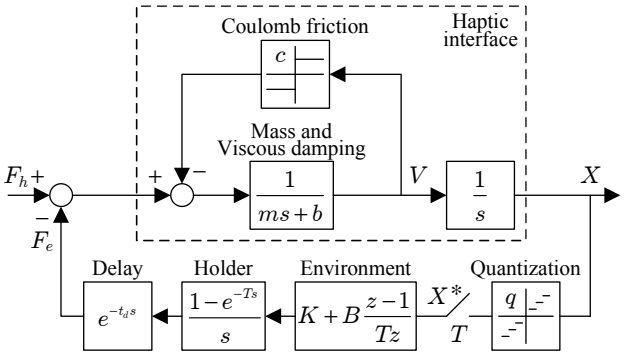

Fig. 1. Model of a haptic system.

viscoelastic impedance model with stiffness K and damping B is used to compute the force of the environment. It is assumed that the system has no velocity sensor; therefore, the backwards difference is used to estimate velocity. The sampling period is T and the position sensor resolution q.

Some phenomena are not taken into account (possible saturation and quantization in the actuators, internal vibration modes of the interface, etc.). Although the dynamics of the user is also involved in the loop, his influence makes the system more stable [7], [8]. Therefore, he has not been included in the block diagram.

A simplified model of the system is shown in Fig. 2. Since this model contains only linear phenomena, it is valid if the Coulomb friction and the quantization are negligible. Moreover, since in [8] and [9] was found that the Coulomb friction can dissipate the energy introduced by the quantization, it is interesting to use the linear model as "worst case" to find stability conditions.

Following [10], the dimensionless parameters that will be used in this paper are shown in Table I. Although some authors [8] have used the virtual stiffness to normalize the parameters, we prefer to use the mass (or the inertia for rotary degrees of freedom), because this way the values of the device do not change with the contact force law.

Both real and dimensionless parameters can theoretically take any value ($m > 0$, $b > 0$, $T > 0$ and $t_d \geq 0$). However, typical sampling rates in haptics are quite fast ($\geq$ 1 kHz)

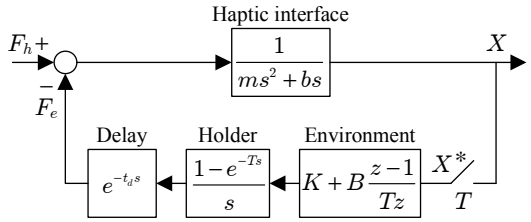

Fig. 2. Linear model of a haptic system.

TABLE I
DIMENSIONLESS PARAMETERS

Parameter	Variable	Dimensionless variable
Sampling period	T	-
Mass	m	-
Physical damping	b	$\delta = \frac{bT}{m}$
Virtual stiffness	K	$\alpha = \frac{KT^2}{m}$
Virtual damping	B	$\beta = \frac{BT}{m}$
Delay	t_d	$d = \frac{t_d}{T}$

and the relation between the physical damping and the mass cannot be supposed to be arbitrarily large. For example, some experimentally acquired values given in [8] show that $\frac{b}{m} \ll 1\ \mathrm{s}^{-1}$ for all investigated haptic devices. Therefore, the dimensionless physical damping δ should be quite small in haptic systems. In this paper we will suppose that $\delta < 10^{-3}$. As shown later, some conclusions of this paper can only be stated assuming this fact.

III. PREVIOUS ANALYSES

A. Stability approaches

Classical control tools have been applied to the linear system in order to obtain the stability conditions. In [7] it was stated that, with no delay, $d = 0$, the stability condition of the linear system (using the dimensionless parameters of Table I) is

$$\alpha < \delta(\delta+\beta)\frac{(1-\epsilon)(\beta\epsilon+\beta\delta\epsilon-\beta+\delta^2)}{(1-\epsilon-\delta\epsilon)(\beta\epsilon+\beta\delta-\beta+\delta^2)}, \quad (1)$$

where ϵ is a dimensionless number,

$$\epsilon = e^{-\frac{bT}{m}} = e^{-\delta}. \quad (2)$$

Stability condition (1) is consistent with [11]. Substituting ϵ (2) with its Taylor approximation,

$$\epsilon = 1-\delta+\frac{1}{2}\delta^2-\frac{1}{6}\delta^3+O(\delta^4), \quad (3)$$

makes it possible to linearize (1) around the origin and to obtain the following more compact stability condition [7]:

$$\alpha < 2(\delta+\beta). \quad (4)$$

The fact that the dimensionless physical damping δ is a very small number enforces the validity of this approximation. Stability condition (4) was also experimentally found in [12]. Further experimental studies confirm the result that increasing both the physical viscous damping—i.e. electrically [13], [14] or magnetically [15]—and the virtual damping [16], [17] allows for larger stable stiffness coefficients.

If the system contains a delay of one sampling period, $d = 1$, the stability condition that has been proposed in [18] using the Padé approximation is

$$\alpha < \frac{2}{3}(\delta+\beta). \quad (5)$$

B. Passivity approaches

Another way to guarantee the stability of the system is ensuring its passivity [19]. The passivity condition for the linear system without delay proposed by Colgate [20] is

$$\alpha < 2(\delta-|\beta|). \quad (6)$$

The influence of the virtual damping on the passivity condition differs from the stability one (4) for $\beta > 0$. Since passivity is a more restrictive condition than stability, the passive region in the (α,β)-plane is a subregion inside the stable region. However, it is interesting to note that the same condition for both passivity and stability can be obtained if no virtual damping is included.

Passivity analysis has been successfully extended [8] to the non-linear system depicted in Fig. 1, but without including the effect of the virtual damping β. In [9] equivalent results were obtained without the influence of the delay.

IV. STABILITY CONDITION

In this paper, we propose a stability condition for the linear system including the effect of both, delay and virtual damping. Our stability condition may be seen as generalization of previous conditions (4) and (5) for any delay, consistent with the study of the non-linear system [8] but including the effect of the virtual damping β:

$$\alpha < \frac{2}{1+2d}(\delta+\beta). \quad (7)$$

Using the physical values of the parameters the proposed stability condition is

$$K < \frac{2}{T+2t_d}(b+B). \quad (8)$$

The validity of this formula will be checked by four different ways: 1) with theoretical analysis, 2) solving numerically the characteristic equation and performing a graphical approach, 3) running simulations, 4) with experimental results.

Rearranging the stability equation which relates the real parameters of the system,

$$K < \frac{b+B}{\frac{T}{2}+t_d}, \quad (9)$$

and taking into account that the effect of the sampling and hold in the control loop can be approximated by a delay of half the sampling period $\frac{T}{2}$, we can interpret our stability condition (7) with the following statement:

$$\text{Critical stiffness} = \frac{\sum \text{Damping}}{\sum \text{Delay}}. \quad (10)$$

The critical stiffness of a haptic system is equal to the overall damping of the mentioned system divided by the total delay of the loop. Therefore, a double viscous damping in the system—physical plus virtual—will allow for a double stiffness; while a double delay in the haptic loop—no matter its nature—will half the maximum stable stiffness.

V. Routh-Hurwitz Analysis

The methodology followed in [7] can be used to receive the analytical stability condition from the characteristic equation of the system. In the Z-domain, this equation consists of a polynomial if the delay t_d is a multiple of the sampling period T (then d takes natural values):

$$\begin{aligned}\delta^2(z-\epsilon)(z-1)z^{d+1} - (1-\epsilon-\delta)(\alpha+\beta)z^2 \\ + \left[(1-\epsilon-\delta\epsilon)(\alpha+\beta) + (1-\epsilon-\delta)\beta\right] z \\ -(1-\epsilon-\delta\epsilon)\beta = 0. \end{aligned} \quad (11)$$

The order of this polynomial (11) increases with d (it is $d+3$) and the use of the Routh-Hurwitz criterion becomes quite complex. In section III the analytical solution of the stability boundary for $d=0$ was presented, (1). The following lines derive the stability condition for a delay that is equal to the sampling period ($d=1$). In this case, the characteristic equation is

$$\begin{aligned}\delta^2 z^4 + (1-\epsilon)\delta^2 z^3 + \left[\epsilon\delta^2 - (1-\epsilon-\delta)(\alpha+\beta)\right] z^2 \\ + \left[(1-\epsilon-\delta\epsilon)(\alpha+\beta) + (1-\epsilon-\delta)\beta\right] z \\ -(1-\epsilon-\delta\epsilon)\beta = 0. \end{aligned} \quad (12)$$

After the bilinear transformation used in [7] it is possible to apply the Routh-Hurwitz criterion and identify the most restrictive condition. This exact condition for stability is

$$a_1 a_2 a_3 - a_4 a_1^2 - a_3 a_0^2 > 0, \quad (13)$$

where:

$$\begin{aligned} a_0 &= (1-\epsilon)\tfrac{\delta\alpha}{2}, \\ a_1 &= (1-\epsilon)(\delta\beta + \delta^2 - \alpha) + \epsilon\delta\alpha, \\ a_2 &= (1-\epsilon)(\alpha - 2\beta) + \delta(3\delta - \epsilon\delta + 3\beta\epsilon - \beta - \alpha), \\ a_3 &= (1-\epsilon)(\alpha + 4\beta) + \delta(3\delta + \epsilon\delta - 3\beta\epsilon - \beta - \epsilon\alpha), \\ a_4 &= -(1-\epsilon)(\alpha + 2\beta) + \tfrac{\delta}{2}(1+\epsilon)(\alpha + 2\beta + 2\delta). \end{aligned}$$

It is not possible to isolate parameter α as it was done in (1) because some powers of this parameter appear in (13).

Fig. 3 shows the stability boundaries using analytical conditions (1) and (13), for small dimensionless physical damping ($\delta < 10^{-3}$). Taking different values of δ within this range, it is quite difficult to appreciate any change in the overall shape of the stability boundaries. Therefore, their maximum values $\alpha_{max}^{d=0} \approx 0.686$ and $\alpha_{max}^{d=1} \approx 0.144$ can be taken as constants, [21].

As could be expected, the stability region with delay is smaller than the stability region without delay.

Although it has been stated that the overall shape of the stability boundaries depicted in Fig. 3 nearly does not change with δ, it is possible to detect some little but important differences for relatively small values of β. Fig. 4 summarizes this behavior (it is a zoom of Fig. 3 near the point of origin).

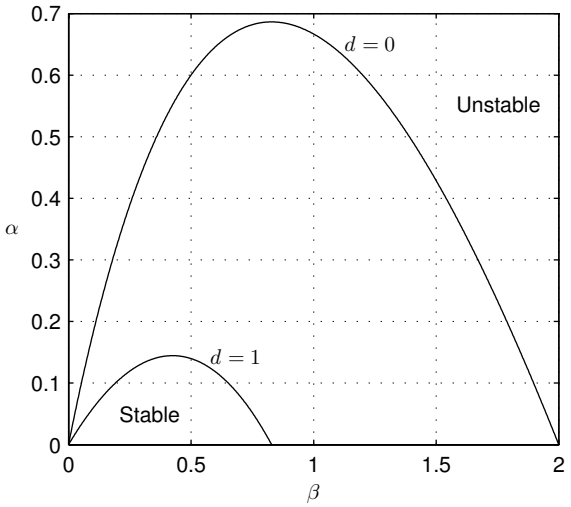

Fig. 3. Stability boundaries using the analytical conditions, for small dimensionless physical damping ($\delta < 10^{-3}$), without delay ($d=0$) and with a delay equal to the sampling period ($d=1$).

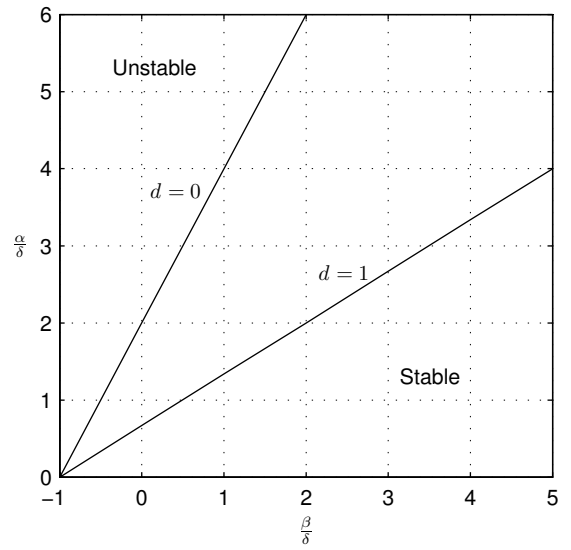

Fig. 4. Zoom of the stability boundaries using the analytical conditions, for small dimensionless physical damping ($\delta < 10^{-3}$), without delay ($d=0$) and with a delay equal to the sampling period ($d=1$).

The stability boundaries start at a virtual damping equal to the negative physical one ($\beta = -\delta$); so it is possible to introduce a negative virtual damping up to this value.

Substituting the Taylor approximation (3) in stability condition (13), yields

$$\alpha < \frac{2}{3}(\delta + \beta), \quad (14)$$

where it was possible to isolate parameter α. This condition fits the beginning of the corresponding stability boundary in Fig. 4 and also confirms previous result (5) which was obtained with different approximations and confirmed with experimental results.

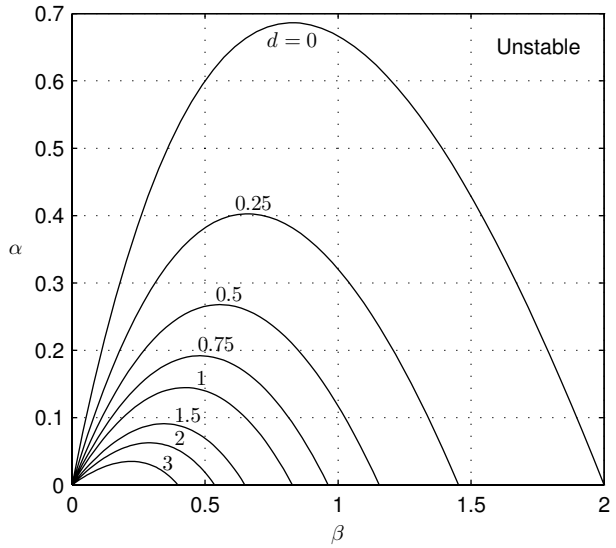

Fig. 5. Stability boundaries for small dimensionless physical damping ($\delta < 10^{-3}$) and delays $d = [0, 0.25, 0.5, 0.75, 1, 1.5, 2, 3]$.

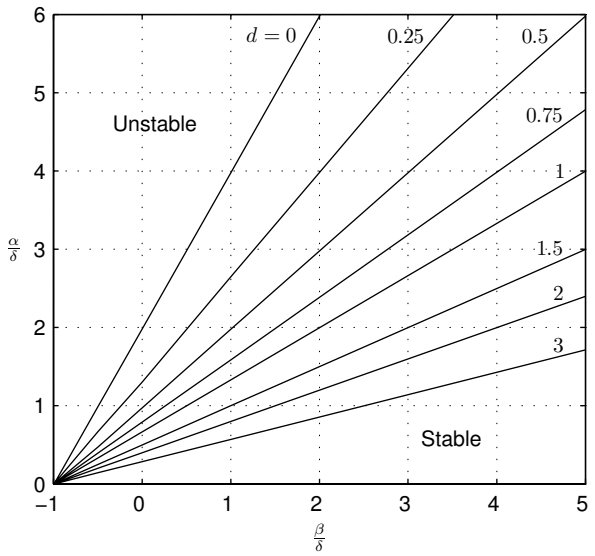

Fig. 6. Zoom of the stability boundaries near the point of origin for small dimensionless physical damping ($\delta < 10^{-3}$) and delays $d = [0, 0.25, 0.5, 0.75, 1, 1.5, 2, 3]$.

VI. Graphical Analysis

The validity of (7) is checked in this section using the graphs of the stability boundaries. Two different ways have been used to obtain and depict the critical stiffness of the linear system with delay. The first one follows [7] and directly obtains the critical stiffness for different values of the virtual damping evaluating

$$\alpha < \text{Gm}\left[\frac{1}{\frac{z^d(z-1)(z-\epsilon)\delta^2}{(\epsilon-1+\delta)z+1-\epsilon-\delta\epsilon}+\beta\frac{z-1}{z}}\right], \qquad (15)$$

where Gm[.] means gain margin of the Z-transfer function. The second method, used in [10] and [22], numerically solves the poles of the characteristic equation (11) and finds the stiffness coefficients which place all the poles just within the unit circle.

Although both methods obtain the same results, the gain margin can be computed easily in Matlab® only if the delay is a multiple of the sampling period T, while the other method allows for introducing fractional numbers for the delay. Fig. 5 shows the stability boundaries for different delays d and setting $\delta < 10^{-3}$; while Fig. 6 shows a zoom of Fig. 5 near the point of origin.

The shown boundaries in Fig. 6 fit perfectly the linearized stability condition (7),

$$\alpha < \frac{2}{1+2d}(\delta+\beta). \qquad (16)$$

The initial slope of the stability boundaries becomes smaller with the delay. Therefore, the critical stiffness without virtual damping $\beta = 0$ decreases also with the delay. This means that, using the physical parameters, the critical stiffness depends on both the physical damping and the delay.

Notice that this result is a graphical analysis which just shows the consistency of (7). It can be only considered as a proof after showing that it fits the exact analytical conditions, like the ones presented in the previous section for $d = 0$ and $d = 1$.

VII. Simulation Results

Many simulations have been performed to check stability condition (8); however, since all of them hold that condition only few of them are shown in this paper. Table II shows the critical virtual stiffness, for several values of delay and virtual damping. The sampling period was set equal to 1 ms, the mass equal to 1 kg, and the physical damping 0.1 Ns/m.

Simulations show that the virtual damping increases the critical stiffness in the same way as the physical one does. They also confirm that the mass of the interface does not influence the critical stiffness of the system. All the values obtained during the simulations hold well condition (8).

TABLE II

Critical stiffness versus delay and virtual damping, with $m = 1$ kg, $b = 0.1$ Ns/m and $T = 1$ ms

Critical stiffness (N/m)		Virtual damping (Ns/m)			
		0.1	0.2	0.3	0.4
Delay (ms)	0	399.89	599.78	799.75	999.22
	0.25	266.61	399.89	533.17	666.26
	0.5	199.97	299.93	399.89	499.73
	0.75	159.98	239.94	319.91	399.79
	1	133.32	199.95	266.58	333.16
	1.5	99.99	149.97	199.93	249.89
	2	79.99	119.97	159.93	199.89
	3	57.14	85.69	114.23	142.76
	4	44.44	66.64	88.83	111.03

VIII. Experimental Results

The DLR Light-Weight Robot III (Fig. 7) has been used to perform some experiments [23]. Every joint has an internal

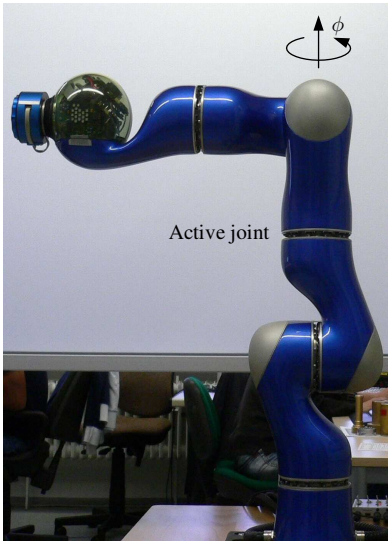

Fig. 7. DLR Light-Weight Robot III.

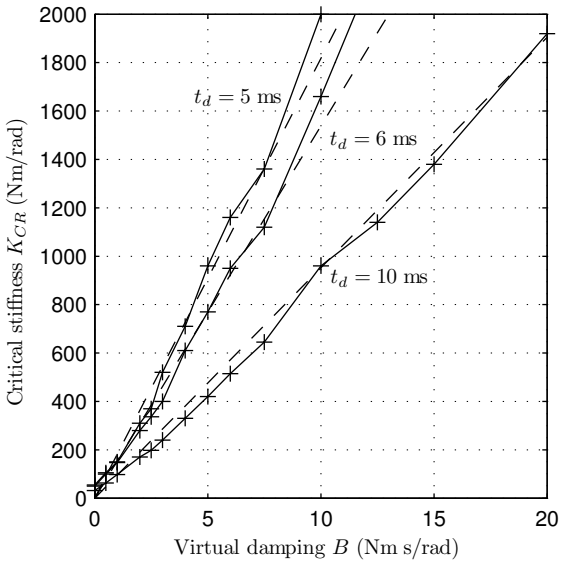

Fig. 8. Experimental stability boundaries for a delay t_d of 5, 6 and 10 ms (pluses and solid); and theoretical boundaries (dashed).

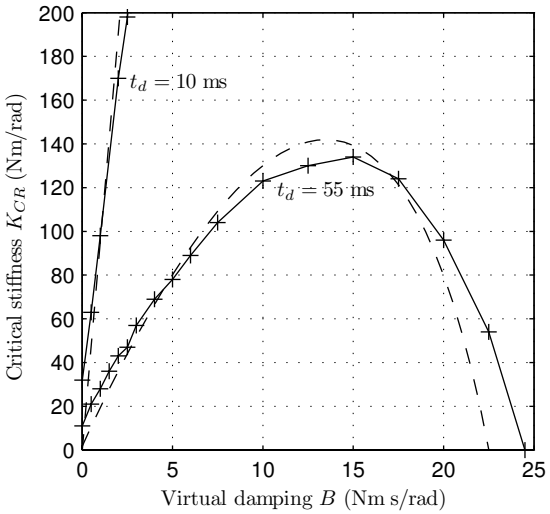

Fig. 9. Experimental stability boundaries for a delay t_d of 10 and 55 ms (pluses and solid); and theoretical boundaries (dashed).

controller which compensates the gravity and the Coulomb friction. Since high-resolution position sensors are used to measure the link orientations (quantization $q \approx 20$"), non-linear effects can be neglected.

A bilateral virtual wall consisting of a virtual spring and damper was implemented in the third axis of the robot (rotating angle ϕ in Fig. 7). Limit stable parameter values were obtained when sustained oscillations were observed increasing the stiffness. The environment was implemented using a computer connected via Ethernet to the robot. The sampling rate was 1 kHz and the overall loop contained a delay of 5 ms. No user was involved in the experiments. Fig. 8 shows the experimental results introducing several fixed values for the virtual damping. A set of experiments was performed with only the system delay of 5 ms, while additional delays were artificially introduced in the loop to obtain an overall delay of 6 and 10 ms. The theoretical behavior is depicted with dotted lines. The experimental stability boundaries fit very well the linear condition.

A very large delay was also introduced in the system in order to receive a curved stability boundary. Fig. 9 shows the experimental stability boundary for an overall delay of 55 ms. The beginning of the stability boundary for a delay of 10 ms is also shown in the same figure. The theoretical stability curve has been computed using an inertia of the device in the configuration selected for the experiments: 0.8 kg·m^2.

IX. Valid Range of the Linear Condition

The shape of the stability boundary can be divided into two different parts. The first one follows the linear condition (8) for relatively small values of virtual damping (Fig. 6). The second one is a curve (Fig. 5) which only can be obtained graphically—although we know the exact analytical conditions of two cases: without delay (1) and with a delay of one sampling period (13). In this section we discuss the frontier between these two parts.

Fig. 10 shows the points in which the relative error of the linearization (8) to the exact boundaries is 2% and 5% for the two cases $\delta = 0$ and $\delta = 0.01$. Obviously, the linear condition (8) presented in this paper can be used even for high physical damping $\delta = 0.01$; for this value the 2% error is only violated for delay $d \geq 3$ from the beginning.

Regarding the delay, several factors like computation of the collision detection algorithms for complex virtual environments, digital to analog conversion, amplifier dynamics, etc. introduce a certain delay in the haptic system that is usually equal to or less than one sampling period, $d \leq 1$, [8]. Therefore, the linear condition (8) holds quite well for haptic devices. In other kind of systems, which usually involve longer delays (i.e. in teleoperated systems it is quite common to suppose a delay equal to hundreds of ms), the linear stability condition should not be used.

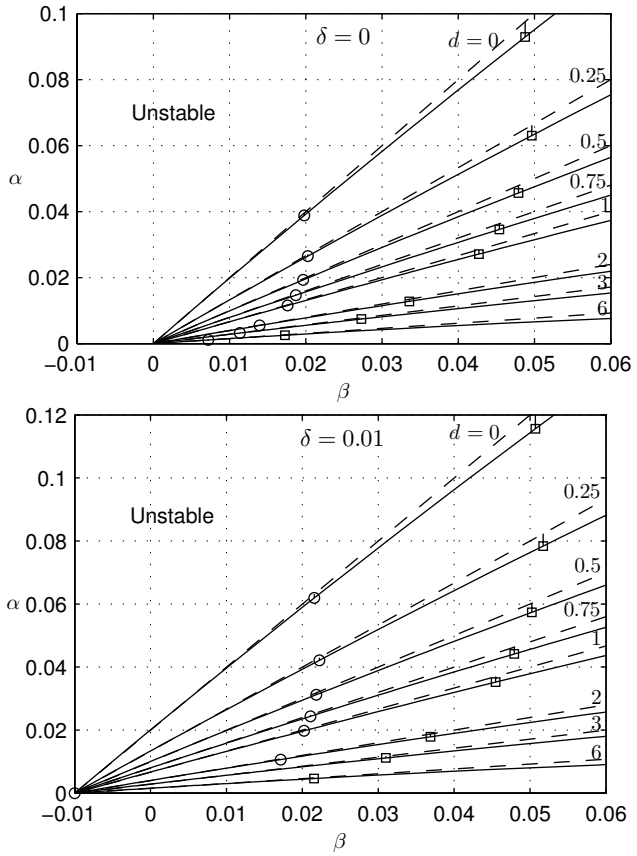

Fig. 10. Exact stability boundaries (solid) for different delays and places where the relative error of the linear condition (8) (dashed) is equal to 2% (circles) and equal to 5% (squares) for $\delta = 0$ and $\delta = 0.01$.

X. Conclusions and Future Work

This paper studies the influence of the viscous damping and the delay in the stability of haptic systems. The stability boundaries have been found by means of different approaches: 1) analytically using the Routh-Hurwitz criteria; 2) numerically computing the poles of the characteristic equation, 3) performing simulations and 4) experimentally.

Although analytical expressions of the stability boundaries are quite complex, a linear condition between stiffness, damping and system delay can be used for haptic systems. This condition is independent of the mass of the device. Furthermore, it seems that the virtual and the physical damping have the same influence on the system inside the valid range of the linear condition. Thus, in combination with the delay the virtual spring causes energy gain [24], and not the virtual damping. Comparing the linear stability condition to the exact boundary demonstrates that it is valid for a wide parameter range of the virtual environment. Yet, since the analyses presented in this paper assume the linearity of the system, its results can only be taken as an approximation if non-linear phenomena (like Coulomb friction and sensor resolution) are not negligible.

For future work it would be interesting to investigate these nonlinear effects. Also examining the robustness against uncertain physical parameters and external disturbances is worthful.

References

[1] E. Chen, "Six degree-of-freedom haptic system for desktop virtual prototyping applications," in *First International Workshop on Virtual Reality and Prototyping*, Laval, France, 1999, pp. 97–106.

[2] J. Savall, D. Borro, J. J. Gil, and L. Matey, "Description of a haptic system for virtual maintainability in aeronautics," in *IEEE/RSJ Int. Conf. Intelligent Robots Systems*, Lausanne, Switzerland, 2002, pp. 2887–2892.

[3] T. Hulin, C. Preusche, and G. Hirzinger, "Haptic rendering for virtual assembly verification," in *World Haptics Conf.*, Pisa, Italy, 2005.

[4] A. J. Madhani, G. Niemeyer, and J. K. Salisbury, "The black falcon: A teleoperated surgical instrument for minimally invasive surgery," in *IEEE/RSJ Int. Conf. Intelligent Robots Systems*, Victoria B.C., Canada, 1998, pp. 936–944.

[5] M. Li and Y.-H. Liu, "Haptic modeling and experimental validation for interactive endodontic simulation," in *IEEE Int. Conf. Robotics and Automation*, Orlando, Florida, USA, 2006, pp. 3292–3297.

[6] W.-S. Lee, J.-H. Kim, and J.-H. Cho, "A driving simulator as a virtual reality tool," in *IEEE Int. Conf. Robotics and Automation*, Leuven, Belgium, 1998, pp. 71–76.

[7] J. J. Gil, A. Avello, A. Rubio, and J. Flórez, "Stability analysis of a 1 dof haptic interface using the routh-hurwitz criterion," *IEEE Trans. Control Syst. Technol.*, vol. 12, no. 4, pp. 583–588, 2004.

[8] N. Diolaiti, G. Niemeyer, F. Barbagli, and J. K. Salisbury, "Stability of haptic rendering: Discretization, quantization, time-delay and coulomb effects," *IEEE Trans. Robot.*, vol. 22, no. 2, pp. 256–268, 2006.

[9] J. J. Abbott and A. M. Okamura, "Effects of position quantization and sampling rate on virtual-wall passivity," *IEEE Trans. Robot.*, vol. 21, no. 5, pp. 952–964, 2005.

[10] T. Hulin, C. Preusche, and G. Hirzinger, "Stability boundary for haptic rendering: Influence of physical damping," in *IEEE/RSJ Int. Conf. Intelligent Robots Systems*, Beijing, China, 2006.

[11] R. B. Gillespie, "Haptic display of systems with changing kinematic constraints: The virtual piano action," Ph.D. Thesis, Stanford University, 1996.

[12] M. Minsky, M. Ouh-young, O. Steele, F. Brooks Jr., and M. Behensky, "Feeling and sensing: Issues in force display," *Comput. Graph.*, vol. 24, no. 2, pp. 235–243, 1990.

[13] J. S. Mehling, J. E. Colgate, and M. A. Peshkin, "Increasing the impedance range of a haptic display by adding electrical damping," in *First WorldHaptics Conf.*, Pisa, Italy, 2005, pp. 257–262.

[14] L. J. Tognetti and W. J. Book, "Effects of increased device dissipation on haptic two-port network performance," in *IEEE Int. Conf. Robotics and Automation*, Orlando, Florida, USA, 2006, pp. 3304–3311.

[15] A. H. Gosline, G. Campion, and V. Hayward, "On the use of eddy current brakes as tunable, fast turn-on viscous dampers for haptic rendering," in *Eurohaptics Conf.*, Paris, France, 2006.

[16] J. E. Colgate and J. M. Brown, "Factors affecting the z-width of a haptic display," in *IEEE Int. Conf. Robotics and Automation*, vol. 4, San Diego, CA, 1994, pp. 3205–3210.

[17] F. Janabi-Sharifi, V. Hayward, and C.-S. J. Chen, "Discrete-time adaptive windowing for velocity estimation," *IEEE Trans. Control Syst. Technol.*, vol. 8, no. 6, pp. 1003–1009, 2000.

[18] B. Bonneton and V. Hayward, "Implementation of a virtual wall," McGill University, Tech. Rep., 1994.

[19] R. J. Adams and B. Hannaford, "Stable haptic interaction with virtual environments," *IEEE Trans. Robot. Autom.*, vol. 15, no. 3, pp. 465–474, 1999.

[20] J. E. Colgate and G. Schenkel, "Passivity of a class of sampled-data systems: Application to haptic interfaces," *J. Robot. Syst.*, vol. 14, no. 1, pp. 37–47, 1997.

[21] T. Hulin, C. Preusche, and G. Hirzinger, "Stability boundary and design criteria for haptic rendering of virtual walls," in *8th International IFAC Symposium on Robot Control*, Bologna, Italy, 2006.

[22] S. E. Salcudean and T. D. Vlaar, "On the emulation of stiff walls and static friction with a magnetically levitated input/output device," *J. Dyn. Syst. Meas. Control-Trans. ASME*, vol. 119, pp. 127–132, 1997.

[23] G. Hirzinger, N. Sporer, A. Albu-Schäffer, M. Hähnle, R. Krenn, A. Pascucci, and M. Schedl, "DLR's torque-controlled light weight robot III - are we reaching the technological limits now?" in *IEEE Int. Conf. on Robotics and Automation*, Washington D.C., USA, 2002, pp. 1710–1716.

[24] C. Basdogan and M. A. Srinivasan, "Haptic rendering in virtual environments," in *Virtual Environments HandBook*, K. M. Stanney, Ed. Lawrence Erlbaum Associates, 2002, pp. 117–134.